14th International Symposium on Turbulence and Shear Flow Phenomena (TSFP14)
Heidelberg, Germany, July 28–31, 2026

PRANDTL NUMBER AND REYNOLDS NUMBER EFFECTS ON PASSIVE SCALAR IN TURBULENT ANNULAR PIPE FLOW USING A STOCHASTIC MODEL

Pei-Yun Tsai
Chair of Numerical Fluid and Gas Dynamics
Brandenburg University of Technology Cottbus-Senftenberg
Siemens-Halske-Ring 15A, 03046 Cottbus, Germany
tsaipeiy@b-tu.de

Marten Klein
Chair of Numerical Fluid and Gas Dynamics
Brandenburg University of Technology Cottbus-Senftenberg
Siemens-Halske-Ring 15A, 03046 Cottbus, Germany
marten.klein@b-tu.de

Heiko Schmidt
Chair of Numerical Fluid and Gas Dynamics
Brandenburg University of Technology Cottbus-Senftenberg
Siemens-Halske-Ring 15A, 03046 Cottbus, Germany
heiko.schmidt@b-tu.de

ABSTRACT

Turbulent concentric annular pipe flow with passive heat transfer is analyzed using the stochastic one-dimensional turbulence (ODT) model, which fully resolves viscous, conductive, and turbulent transport along a radial domain at low computational cost. Simulations are performed for $Pr = 0.71$ and 0.025 over a range of bulk Reynolds number Re_{D_h} values while focusing on radius ratio $\eta = 0.1$. Present results demonstrate a strong influence of curvature on thermal statistics over the two curved walls. The analytical expression for the boundary layer yields results in good agreement with the classical logarithmic wall function. The results indicate that a linear expression is inadequate for representing near-wall statistical features in the conductive domain. Additionally, the log-law region is inadequate when curvature and finite-Reynolds-number effects are not accounted for. The predictive capabilities of ODT are utilized to obtain simplifying, physically based Nusselt number correlations. These findings improve the understanding of scalar transport in annular flows and support the development of curvature-aware wall models and heat exchanger design.

INTRODUCTION

Concentric coaxial (annular) pipe flow is found in various engineering applications, such as coaxial geothermal heat exchangers and photochemical reactors. The investigation of turbulent annular pipe flow is a canonical problem that provides detailed insights into radial transport processes and boundary layers over both convex and concave walls.

Numerous numerical and experimental studies have been carried out to better understand the heat transfer in turbulent annular pipe flows. Key areas of focus include the impact of spanwise curvature between the inner and outer cylindrical walls on the asymmetry of statistical moments in velocity and temperature fields (Boersma & Breugem (2011); Bagheri & Wang (2021)), and the Nusselt number (Kays *et al.* (1980)). The literature indicates that the effects of key physical parameters, such as radius ratio η, Prandtl number Pr, and Reynolds number Re, on heat transfer in annular pipe flows have been widely studied. However, compared with plane channel and circular pipe flows, studies focusing on the thermal boundary layer in annular geometries and its dependence on Pr and Re remain limited. The presence of a curved inner wall further complicates the direct application of the classical logarithmic law of the wall, particularly at small radius ratios (wide-gap configurations). In addition, due to experimental limitations and the high computational cost of direct numerical simulations, data for Nusselt number in fully heated annular flows at high Reynolds number are scarce.

To address these challenges, a stochastic modeling approach based on Kerstein's (1999) one-dimensional turbulence (ODT) model is employed, enabling high resolution simulations at reduced computational cost. In this study, we perform a comparative analysis of thermal transport for $Pr = 0.71$ and 0.025 with small radius ratio $\eta = 0.1$, including first- and second-order thermal statistics. Furthermore, an improved wall function that accounts for the radius ratio in the thermal boundary layer on the spanwise curved walls is proposed.

MODEL FORMULATION

Figure 1 shows the geometry and coordinate system of the concentric annular pipe flow investigated. The coordinates x, r, and θ denote the axial, radial, and azimuthal directions, respectively, while u, v, and w represent the velocity components in these directions. The wedge-like computational domain, the ODT domain, is defined in the radial direction and spans the entire annular gap. The flow state is fully resolved along the

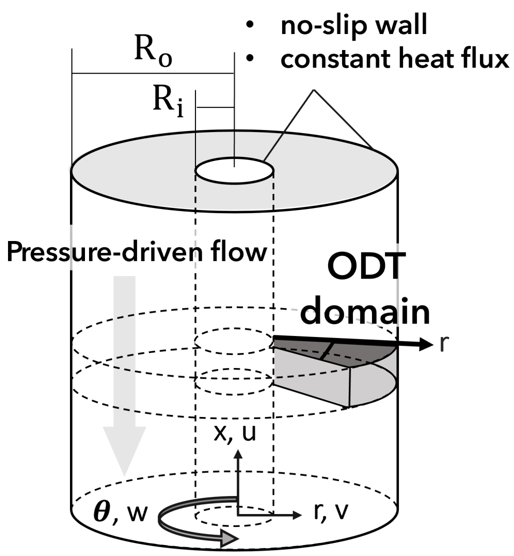

Figure 1. Schematic of the investigated annular pipe flow configuration. The wedge-shaped, radially oriented ODT domain is shown in exaggerated form. No-slip and constant heat flux boundary conditions are prescribed at the inner and outer walls as indicated.

The ODT model, originally developed by Kerstein (1999), is a dimensionally reduced approach designed to capture turbulent transport through a simplified representation of the interaction between advection, viscosity, and scalar diffusion. The model separates molecular diffusion from turbulent advection and resolves all relevant flow scales along a single representative coordinate. Turbulent advection is represented by a stochastic sequence of eddy events, each instantaneously implemented via a physical triplet mapping operation. The location, size, and occurrence rates of eddy events are determined dynamically based on the instantaneous momentum components, but without dependence on passive scalar property fields. Owing to its one-dimensional formulation, ODT achieves significantly lower computational cost while retaining a high level of resolution, resolving boundary layer length scale down to the Kolmogorov or Batchelor scale, comparable to direct numerical simulation (DNS). Although ODT does not replace higher-dimensional approaches such as large eddy simulation (LES) or Reynolds-averaged Navier–Stokes (RANS) methods, ODT is particularly well suited for studying canonical turbulent boundary-layer-type flows.

In the present work, the cylindrical formulation of ODT proposed by Lignell *et al.* (2018) is applied to concentric annular pipe flow. The flow is assumed incompressible and pressure-driven, with no-slip and constant heat-flux boundary conditions imposed at both sides of the walls. Temperature is treated here as a passive scalar. Following the notation of Klein *et al.* (2022), the dimensionally reduced governing equations for momentum and scalar transport can be expressed as

$$\frac{\partial u_i}{\partial t} + \sum_{t_\mathrm{e}} \mathscr{E}_u \, \delta\left(t - t_\mathrm{e}\right) = \frac{1}{r}\frac{\partial}{\partial r}\left(r\nu\frac{\partial u_i}{\partial r}\right) - \frac{1}{\rho}\frac{\mathrm{d}P}{\mathrm{d}x}\,\delta_{ix}\,, \quad (1)$$

$$\frac{\partial \Theta}{\partial t} + \sum_{t_\mathrm{e}} \mathscr{E}_\Theta \, \delta\left(t - t_\mathrm{e}\right) = \frac{1}{r}\frac{\partial}{\partial r}\left(r\alpha\frac{\partial \Theta}{\partial r}\right) + u\,\frac{\mathrm{d}\overline{T}_\mathrm{w}}{\mathrm{d}x}\,. \quad (2)$$

Here, u_i, $i = x, r, \theta$, represents the model-resolved instantaneous velocity vector in cylindrical coordinates, where $u_x = u$, $u_r = v$, and $u_\theta = w$ correspond to the axial, radial, and azimuthal directions, respectively. δ_{ij} is the Kronecker delta, and $\mathrm{d}P/\mathrm{d}x$ denotes the prescribed mean pressure-gradient force density in the axial direction. Under the assumption of statistically stationary annular pipe flow with constant heat flux imposed at both the inner and outer cylindrical walls, the temperature field exhibits a linear increase in the axial direction x. Following Klein *et al.* (2022), the definition of the temperature difference from plane channels is adopted. As discussed in Tsai *et al.* (2023), the influence of wall curvature on the wall temperature is, without loss of generality, compensated by mantle-area-weighting of the wall heat fluxes. The perturbation temperature is defined as $\Theta = \overline{T}_\mathrm{w} - T$, where $\overline{T}_\mathrm{w}$ is the mean wall temperature, which increases linearly with x, and T is the temperature. $\mathrm{d}\overline{T}_\mathrm{w}/\mathrm{d}x$ is therefore the prescribed constant mean streamwise gradient of the wall temperature. The fluid properties, mass density ρ, kinematic viscosity ν, and thermal diffusivity α, are assumed constant. Time is denoted by t, while t_e indicates the stochastically sampled times at which eddy events occur. The Dirac delta function is represented by $\delta(t)$. The terms $\mathscr{E}_u$ and $\mathscr{E}_\Theta$ symbolically represent instantaneous flow profile modifications, which model the instantaneous microstructure modifications with the aid of turbulent advection events. Due to the model's dimensional reduction, an additional pressure fluctuation model is included Kerstein *et al.* (2001), leading to a distinct formulation of $\mathscr{E}_u$ compared to $\mathscr{E}_\Theta$ for a selected turbulent eddy event. Whenever a stochastically sampled eddy event occurs, the radial profiles $u_i(r)$ and $\Theta(r)$ are modified over a selected spatial eddy length scale l_e around a randomly sampled radial eddy location r_e using a mapping procedure. Further details, including the sampling procedure, are skipped here but can be found in Kerstein (1999). For the mesh-adaptive implementation in cylindrical geometry, refer to Lignell *et al.* (2018), and for the treatment of the passive scalar, see Klein *et al.* (2022). The model calibration specific to annular pipe flow follows the model parameters setting in Tsai *et al.* (2023), where the energy distribution parameter $\alpha_\mathrm{odt} = 1/6$, the eddy rate parameter $C_\mathrm{odt} = 5$, and the viscous suppression parameter $Z_\mathrm{odt} = 400$.

For scaling purposes, the

$$u_{\tau,\mathrm{i/o}} = \sqrt{\frac{\tau_\mathrm{i/o}}{\rho}} \quad \text{and} \quad \Theta_{\tau,\mathrm{i/o}} = \frac{\alpha}{u_{\tau,\mathrm{i/o}}}\left|\frac{\mathrm{d}\overline{\Theta}}{\mathrm{d}r}\right|_{\mathrm{wall,i/o}}. \quad (3)$$

Here, $u_{\tau,\mathrm{o/i}}$ denotes the friction velocity at the inner (subscript i) and outer (subscript o) walls, respectively. The wall shear stress, which defines the friction velocity, is expressed as $\tau_\mathrm{i/o} = \mu\,|\mathrm{d}u/\mathrm{d}r|_{\mathrm{wall,i/o}}$, where μ is the dynamic viscosity. $\Theta_{\tau,\mathrm{o/i}}$ represents the friction perturbation temperature at the respective wall.

NUSSELT NUMBER

Heat transfer in annular pipe flow is conventionally characterized using the Nusselt number (Nu), which represents the ratio of convective to purely conductive heat transfer across the fluid domain. This dimensionless number serves as a key indicator of thermal transport efficiency. The bulk Nusselt number, as defined in Fukuda & Tsukahara (2020), is expressed as

$$Nu \equiv \frac{q_w}{\lambda \overline{\Theta}_m / D_h} = \frac{4Re_\tau Pr}{\overline{\Theta}_m^+} . \quad (4)$$

Here, λ denotes thermal conductivity and $\Theta_m^+ = \overline{\Theta}_m / \overline{\Theta}_\tau$ represents the normalized mean perturbation temperature, where $\overline{\Theta}_m$ is the mean perturbation temperature and $\overline{\Theta}_\tau$ is the averaged friction perturbation temperature (due to pressure loss and total heat transfer).

Figure 2 compares the Nusselt number for $Pr = 0.71$ and 0.025 as a function of bulk Reynolds number, Re_{D_h}, for two radius ratios, $\eta = 0.1$ and 0.7. At higher Reynolds numbers, the modeled Nusselt numbers tend to align more closely with the empirical correlation for both Prandtl numbers. For $Pr = 0.71$, the Nusselt number follows the expected monotonic increase with Reynolds number and remains slightly above the empirical predictions, likely due to curvature effects not accounted for in planar-based correlations. In contrast, for $Pr = 0.025$, the dependence on Reynolds number deviates from a linear trend. Furthermore, the difference in Nusselt number between $\eta = 0.1$ and $\eta = 0.7$ decreases with increasing Reynolds number, indicating a reduced sensitivity to curvature at higher Re_{D_h}.

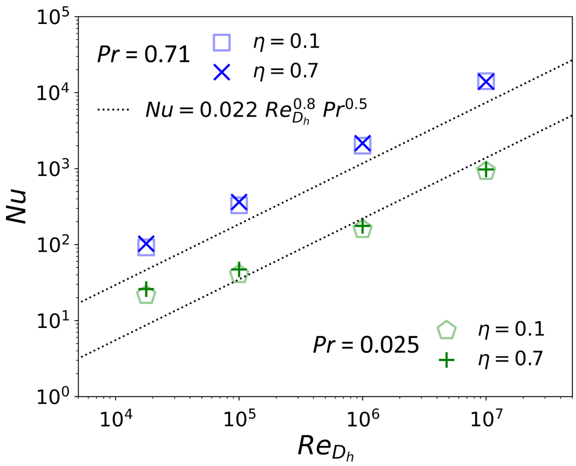

Figure 2. Nusselt number, Nu, as a function of bulk Reynolds number, $Re_{D_\mathrm{h}} = 17700$, 10^5, 10^6, and 10^7. Results are shown for $Pr = 0.71$ and 0.025 and for radius ratios $\eta = 0.1$ and 0.7. The power-law correlation from Kays *et al.* (1980) is included for reference.

MEAN TEMPERATURE PROFILE

Figure 3 presents the mean perturbation temperature profiles predicted by the ODT model for $Pr = 0.71$ and 0.025. In the Prandtl number $Pr = 0.71$ case, the ODT predictions agree closely with the reference DNS data from Bagheri & Wang (2021), with 4% overestimation of the magnitude of the peak temperature. In the low Prandtl number case, $Pr = 0.025$, thermal diffusivity dominates kinematic viscosity, leading to more efficient heat transport than momentum transport. As a result, thermal fluctuations induced by turbulence are more rapidly smoothed out, leading to a faster relaxation toward the purely conductive solution by increased dissipation of turbulence-induced temperature fluctuations. In both cases, wall-curvature effects are clearly evident. The temperature distribution exhibits pronounced asymmetry across the radial gap, reflecting the influence of spanwise curvature on thermal transport. The peak of the mean perturbation temperature is shifted toward the inner wall, where curvature is stronger, resulting in a thinner thermal boundary layer at the inner wall (indicated by a steeper gradient) and a thicker one at the outer wall (indicated by a shallower gradient).

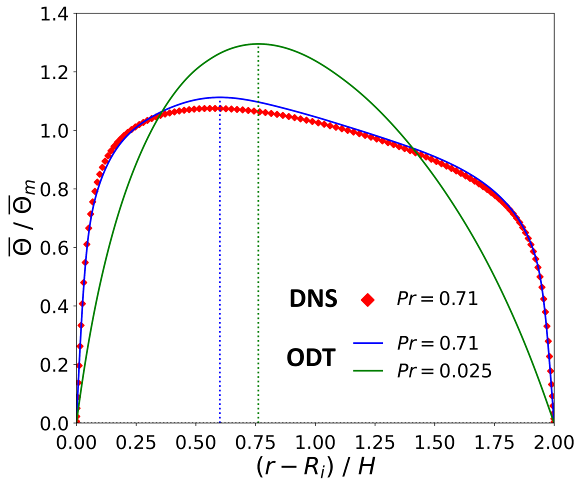

Figure 3. Mean perturbation temperature profiles, normalized by the bulk mean temperature $\overline{\Theta}_\mathrm{m}$, for $Pr = 0.71$ and 0.025 at fixed radius ratio $\eta = 0.1$ and bulk Reynolds number $Re_{D_\mathrm{h}} = 17700$. Reference DNS data from Bagheri & Wang (2021) are included for comparison.

Thermal boundary layer

Figure 4 shows mean temperature profiles across the thermal boundary layer at the inner and outer cylinder walls for both Prandtl numbers. The normalized mean perturbation temperature is defined as $\overline{\Theta}^+ = \overline{\Theta} / \Theta_{\tau,\mathrm{o/i}}$ at the outer and inner walls, respectively, with the corresponding wall-normal coordinate $r^+ = |r - R_{\mathrm{o/i}}|, u_{\tau,\mathrm{o/i}} / \nu$. As anticipated from Figure 3, the $Pr = 0.025$ case exhibits lower magnitudes due to reduced near-wall temperature gradients.

For $Pr = 0.71$, a logarithmic region is observed on the outer wall beginning at $r^+ \approx 30$, following a log-law, $\overline{\Theta}^+ = \frac{1}{\kappa_\Theta} \ln\left(r^+\right) + B_\Theta^+$, characterized by $\kappa_\Theta = 0.35$ and $B_\Theta = 1.34$ from Bagheri & Wang (2021). Overall, the thermal boundary layer is reasonably described by a linear conductive sublayer combined with a logarithmic region, consistent with the classical law of the wall. However, this simplified approach does not fully capture the behavior on the inner cylinder wall, where deviations from the expected behavior are more pronounced. These discrepancies highlight the influence of curvature and its interaction with thermal transport, which will be further discussed in the following thermal boundary layer analysis, based on and extending the work of Boersma & Breugem (2011).

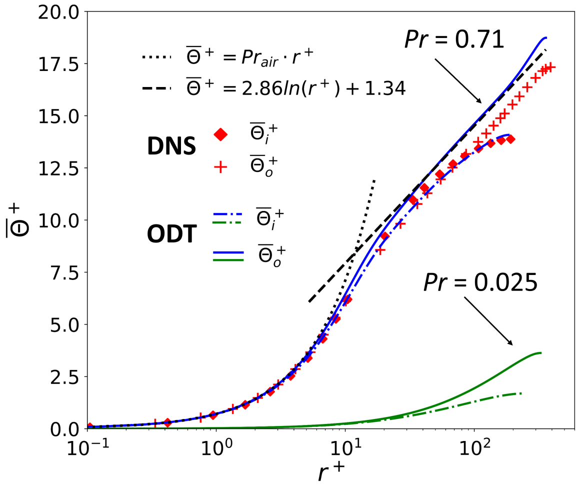

Figure 4. Boundary layer profiles of the mean perturbation temperature at both the inner and outer cylinder walls for $Pr = 0.71$ and 0.025, at fixed $\eta = 0.1$ and $Re_{D_\mathrm{h}} = 17700$. Reference DNS data from Bagheri & Wang (2021) is shown for comparison.

CONDUCTIVE-DOMINATED REGION

Assuming a fully developed flow, all statistical properties remain constant in both the axial and azimuthal directions. As a result, only the steady-state balance equations governing the radial variation of the flow's statistical moments need to be considered. Applying the Reynolds-averaging procedure to Equation (2), followed by rearrangement and a single integration over the radial coordinate r, yields the heat flux balance equation as

$$\overline{\Theta' v'} - \alpha \frac{\mathrm{d}\overline{\Theta}}{\mathrm{d}r} = r\overline{u}\,\frac{\mathrm{d}\overline{T}_\mathrm{w}}{\mathrm{d}x} + \frac{C_1}{r}\,, \qquad (5)$$

$$C_1 = \frac{1}{\rho\, C_p}\,\frac{q_\mathrm{i}\, R_\mathrm{o} - q_\mathrm{o}\, R_\mathrm{i}}{R_\mathrm{i}/R_\mathrm{o} - R_\mathrm{o}/R_\mathrm{i}}\,. \qquad (6)$$

Here, C_1 is an integration constant that can be expressed in terms of the heat fluxes at the inner and outer cylindrical walls. C_p is the heat capacity of the fluid at constant pressure, q_i and q_o are the constant wall heat fluxes at the inner and outer cylinder walls, respectively.

Figure 5(b) presents the distribution profiles of normalized heat fluxes, including the conductive (molecular) heat flux defined by $q_\mathrm{con} = -\alpha\left(\mathrm{d}\overline{\Theta}/\mathrm{d}r\right)$, the turbulent heat flux arising from velocity and temperature fluctuations given by $q_\mathrm{tur} = \overline{\Theta' v'}$, and the total heat flux, calculated as $q_\mathrm{tot} = q_\mathrm{con} + q_\mathrm{tur}$. It is observed that there is a clear separation between the regions dominated by conductive and turbulent thermal transport. The conductive heat flux governs the heat transport near the wall, and the turbulent heat flux becomes the primary contributor to heat transport for $r^+ > 20$.

In the region very close to the wall, which is the conductive-dominated region, the conductive term, $\alpha\left(\mathrm{d}\overline{\Theta}/\mathrm{d}r\right)$, significantly outweighs the turbulent transport term, $\overline{\Theta' v'}$. Assuming conduction dominates, meaning that $\overline{\Theta' v'} \ll \alpha\left(\mathrm{d}\overline{\Theta}/\mathrm{d}r\right)$, and considering small but finite radius ratios ($\eta \ll 1$), the normalized form of Equation (5) in friction units can be simplified to

$$\overline{\Theta}^+(r^+) = Pr\, R_\mathrm{i}^+ \ln\left(\frac{r^+ + R_\mathrm{i}^+}{R_\mathrm{i}^+}\right)\,. \qquad (7)$$

Here, $R_\mathrm{i}^+ = (R_\mathrm{i}\, u_{\tau,\mathrm{i}})/\nu$ is not a constant, but a parameter that depends on the wall geometry and the state of the turbulent flow, meaning that it depends on the curvature radius and the wall-shear stress at the cylindrical inner wall. A parameterization of R_i^+ would be needed for wall modeling to provide closure over a strongly curved wall by prescribing the behavior of low-order statistical moments. It is observed that the region near the wall does not follow a purely linear behavior as in the classical law of the wall.

MIXING-LENGTH-DOMINATED REGION

The same approach described above is applied to the regions dominated by turbulent thermal transport, which is mixing-length-dominated region. The difference is that a mixing total heat flux is now assumed to be predominantly transported by turbulent heat flux, such that $\alpha\left(\mathrm{d}\overline{\Theta}/\mathrm{d}r\right) \ll \overline{\Theta' v'}$. For small radius ratios ($\eta \ll 1$), the integration constant C_1 can be simplified by considering the large-gap limit, $R_\mathrm{o} \gg R_\mathrm{i}$. For the rest, the radial dependence is kept in place. To model the turbulent transport term, a gradient-flux approximation is employed: $\overline{\Theta' v'} \simeq -\alpha_t\left(\mathrm{d}\overline{\Theta}/\mathrm{d}r\right)$. The turbulent thermal diffusivity is therefore defined as $\alpha_t = -\overline{\Theta' v'}\big/\left(\mathrm{d}\overline{\Theta}/\mathrm{d}r\right)$, in analogy to the turbulent eddy viscosity $\nu_t = -\overline{u'v'}\big/\left(\mathrm{d}\overline{u}/\mathrm{d}r\right)$. Both α_t and ν_t contribute to the definition of the turbulent Prandtl number, $Pr_t = \nu_t/\alpha_t$. The eddy viscosity ν_t can be parameterized using mixing-length theory in full analogy to Boersma & Breugem (2011), while α_t can subsequently be determined using the Reynolds analogy, provided Pr_t is known from empirical data. Figure 5(c) presents the wall-normal distribution of the turbulent Prandtl number, Pr_t, obtained from ODT. For the prediction of the temperature profile in the mixing-length-dominated region, based on boundary layer theory, a turbulent profile is identified and the mixing-length-dominated region is described by almost constant $Pr_t \simeq 0.95$ for $Pr = 0.71$ case and $Pr_t \simeq 1.3$ for $Pr = 0.025$ case (profiles not shown due to manuscript length constraints).

An expression for the turbulent eddy viscosity was previously proposed by Boersma & Breugem (2011), taking the form $\nu_t = \varepsilon_1 \sqrt{\tau_\mathrm{i}/\rho}\,(r - R_\mathrm{i})$, where ε_1 is an unknown proportionality constant that must be determined from data. This mixing-length formulation implies the presence of nonlocal curvature effects, influencing both the conductive sublayer and the logarithmic region of the thermal boundary layer near the cylindrical inner wall. Most importantly, it is suggested that turbulent eddy sizes do not scale linearly with wall distance, but instead scale with the square root of the distance from the curved surface. This scaling can be motivated both physically and mathematically by enforcing area (measure) conservation during the radial displacement of fluid parcels in an incompressible, constant-property flow. Although these arguments were not explicitly elaborated in Boersma & Breugem (2011), the mathematical implications for model well-posedness were discussed. Regardless, the mixing-length model remains consistent with the underlying flow physics, as confirmed by their DNS data. Substituting the mixing-length expression into Equation (5), followed by normalization using friction units, yields the mean perturbation temperature profile as

$$\overline{\Theta}^{+}(r^{+}) = \frac{Pr_t}{\varepsilon_1^{+}} \ln\left(\frac{r^{+}}{r^{+}+R_\mathrm{i}^{+}}\right) + D_1^{+} \,. \tag{8}$$

Here, ε_1^{+} and D_1^{+} are parametrization coefficients that can be determined from the ODT simulation data. The resulting mean perturbation temperature profile follows a logarithmic form with a shifted argument that explicitly depends on the Reynolds number. This dependence implies that a universal master profile does not exist for walls with significant spanwise curvature, which marks a clear departure from the classical law-of-the-wall on planar or weakly curved surfaces.

Figure 5(a) shows the development of the thermal boundary layer along the inner cylinder wall for Reynolds numbers ranging from $Re_{D_\mathrm{h}} = 17700$ to 10^6. The results are compared for $Pr = 0.71$ and 0.025, at a fixed radius ratio of $\eta = 0.1$. The ODT simulation results are presented alongside the theoretical profiles derived from Equations (7) and (8). The corresponding values of the coefficients ε_1^{+} and D_1^{+} for each case are summarized in Table 1.

In the conduction-dominated region, Equation (7) provides an excellent representation of the near-wall temperature profile, as evidenced by the collapse of all data onto a single master curve. In the mixing-length-dominated region, Equation (8) captures the essential statistical features of the thermal boundary layer at the inner wall over a wide range of Reynolds numbers. Notably, for the low-Prandtl-number case ($Pr = 0.025$), the model remains effective despite the dominance of conductive heat transport, giving a physically based representation of the overall thermal field in terms of radial perturbation temperature profiles. This demonstrates the robustness of the boundary-layer theory for finite Reynolds numbers, beyond its nominal range of applicability to high asymptotic Reynolds numbers. Moreover, for $Pr = 0.025$, a distinct logarithmic region in the temperature profile becomes increasingly evident at high Reynolds numbers ($Re_{D_\mathrm{h}} > 10^5$), which confirms previous results from Ould-Rouiss *et al.* (2010).

Table 1. Coefficients in Equation (8) for three test cases with fixed $\eta = 0.1$ varying the bulk Reynolds number.

	$Pr = 0.71$		$Pr = 0.025$	
Re_{D_h}	ε_1^{+}	D_1^{+}	ε_1^{+}	D_1^{+}
17700	0.227	15.577	1.002	1.987
10^5	0.274	19.141	0.562	4.948
10^6	0.245	24.645	0.401	10.631

TURBULENT HEAT FLUX

Figure 6 presents the radial turbulent heat flux, $-\overline{v'\Theta'}^{+}$, for Prandtl numbers $Pr = 0.71$ and 0.025 at $\eta = 0.1$ and $Re_{D_\mathrm{h}} = 17700$. For $Pr = 0.71$, the result shows good agreement with reference DNS, indicating that ODT is able to adequately capture the geometry effects. The radial profiles exhibit clear asymmetry, similar to that observed in Reynolds shear stress (not shown here, see Tsai *et al.* (2026) for details). As expected, the magnitude of the turbulent heat flux is higher for $Pr = 0.71$ than for the low-Prandtl-number case $Pr = 0.025$.

Figure 7 presents the normalized root-mean-square (RMS) temperature fluctuations, Θ^{+}_rms, at the inner and outer cylinder walls. The results indicate that temperature fluctuations are generally more significant near the outer wall than near the inner wall. Moreover, the disparity between the temperature variations at the inner and outer walls becomes more pronounced in regions farther from the walls. Compared with DNS data Bagheri & Wang (2021), ODT underestimates the peak value of the temperature fluctuation at $r^{+} \approx 15$, but still captures the spatial scales and overall trend of the fluctuation profiles. For the low-Prandtl-number case ($Pr = 0.025$), although no DNS reference is available, the ODT predictions remain physically consistent, exhibiting reduced fluctuation levels relative to the $Pr = 0.71$ case due to enhanced thermal diffusivity.

CONCLUSION

In this study, turbulent heat transfer and thermal flow features in weakly heated concentric annular Poiseuille flow are investigated using a stochastic model. The focus is on the influence of the Prandtl number and the role of spanwise curvature in the thermal boundary layer at high Reynolds numbers. Simulations were performed with the ODT model and validated against DNS data Bagheri & Wang (2021) at $Re_{D_\mathrm{h}} = 17700$. The heat transfer characteristics are analyzed through the Nusselt number. Results show that curvature effects persist even at high Reynolds numbers, although their impact remains moderate. For $Pr = 0.71$, empirical correlations from Kays *et al.* (1980) reasonably capture both the trend and magnitude of the global Nusselt number. Statistics of turbulent temperature fluctuations are further examined, providing quantitative insight into the influence of geometric (radius ratio) and physical (Re, Pr) parameters. A decrease in Prandtl number from $Pr = 0.71$ to 0.025 leads to reduced near-wall temperature gradients and diminished temperature fluctuation levels. The proposed extension of boundary-layer theory accounts for wall curvature to address limitations of the classical law-of-the-wall. The model remains valid up to $Re_{D_\mathrm{h}} = 10^6$ investigated and robustly extrapolates to a lower Prandtl number with fixed model calibration, demonstrating predictive capabilities relevant for modeling and simulation of heat transfer across working fluids and confinement geometries.

ACKNOWLEDGEMENT

This research is supported by the German Federal Government, the Federal Ministry of Research, Technology and Space and the State of Brandenburg within the framework of the joint project EIZ: Energy Innovation Center (project numbers 85056897 and 03SF0693A) with funds from the Structural Development Act (Strukturstärkungsgesetz) for coal-mining regions.

REFERENCES

Bagheri, Edris & Wang, Bing-Chen 2021 Direct numerical simulation of turbulent heat transfer in concentric annular pipe flows. *Physics of Fluids* **33** (5), 055131.

Boersma, Bendiks Jan & Breugem, Wim-Paul 2011 Numerical simulation of turbulent flow in concentric annuli. *Flow, turbulence and combustion* **86** (1), 113–127.

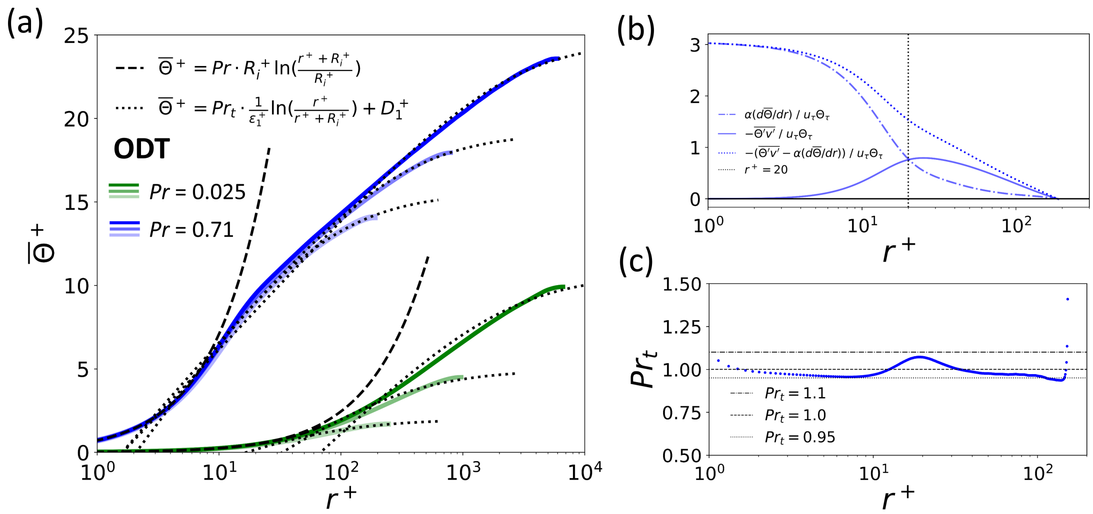

Figure 5. (a) Boundary layer profiles of the mean perturbation temperature at the inner cylinder wall for bulk Reynolds numbers $Re_{D_h} = 17700$, 10^5, and 10^6 (color intensity increasing from light to dark), comparing $Pr = 0.71$ (blue) and 0.025 (green) at fixed radius ratio $\eta = 0.1$. (b) Corresponding distributions of normalized heat flux at the inner wall, and (c) ODT predictions of the turbulent Prandtl number, Pr_t, both for bulk Reynolds number $Re_{D_h} = 17700$ and Prandtl number $Pr = 0.71$ at radius ratio $\eta = 0.1$.

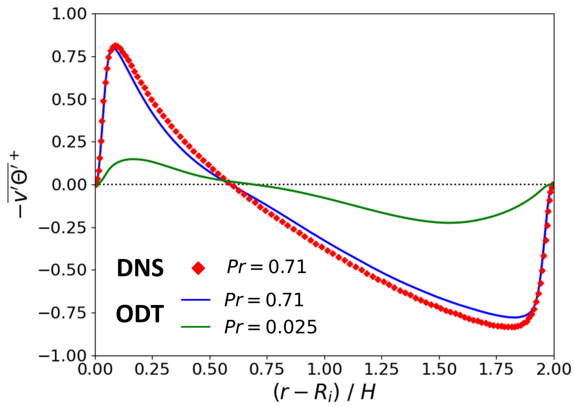

Figure 6. Profiles of the wall-normal turbulent heat flux, $-\overline{v'\Theta'}^+$, comparing $Pr = 0.71$ (blue) and 0.025 (green) at fixed radius ratio $\eta = 0.1$ and $Re_{D_h} = 17700$. Reference DNS data from Bagheri & Wang (2021) is included for comparison.

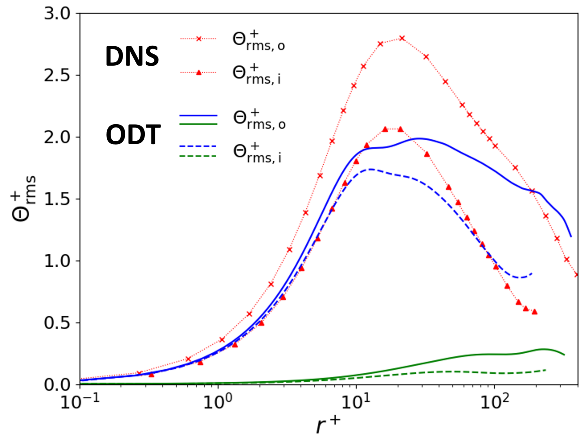

Figure 7. RMS temperature fluctuation profiles Θ^+_{rms} at the inner and outer cylinder walls for $Pr = 0.71$ (blue) and 0.025 (green) at radius ratio $\eta = 0.1$ $Re_{D_h} = 17700$. Reference DNS data is from Bagheri & Wang (2021).

Fukuda, Takehiro & Tsukahara, Takahiro 2020 Heat transfer of transitional regime with helical turbulence in annular flow. *International Journal of Heat and Fluid Flow* **82**, 108555.

Kays, William Morrow, Crawford, Michael E & Weigand, Bernhard 1980 *Convective heat and mass transfer*, , vol. 4. McGraw-Hill New York.

Kerstein, Alan R 1999 One-dimensional turbulence: model formulation and application to homogeneous turbulence, shear flows, and buoyant stratified flows. *Journal of Fluid Mechanics* **392**, 277–334.

Kerstein, Alan R, Ashurst, Wm T, Wunsch, Scott & Nilsen, Vebjorn 2001 One-dimensional turbulence: vector formulation and application to free shear flows. *Journal of Fluid Mechanics* **447**, 85–109.

Klein, Marten, Schmidt, Heiko & Lignell, David O 2022 Stochastic modeling of surface scalar-flux fluctuations in turbulent channel flow using one-dimensional turbulence. *International Journal of Heat and Fluid Flow* **93**, 108889.

Lignell, David O, Lansinger, Victoria B, Medina, Juan, Klein, Marten, Kerstein, Alan R, Schmidt, Heiko, Fistler, Marco & Oevermann, Michael 2018 One-dimensional turbulence modeling for cylindrical and spherical flows: model formulation and application. *Theoretical and Computational Fluid Dynamics* **32** (4), 495–520.

Ould-Rouiss, Meryem, Redjem-Saad, L, Lauriat, Guy & Mazouz, A 2010 Effect of prandtl number on the turbulent thermal field in annular pipe flow. *International communications in heat and mass transfer* **37** (8), 958–963.

Tsai, Pei-Yun, Klein, Marten & Schmidt, Heiko 2026 Numerical simulation of turbulent concentric annular pipe flow using one-dimensional turbulence (odt): Part 1: Momentum transfer. *International Journal of Heat and Fluid Flow* **119**, 110281.

Tsai, Pei-Yun, Schmidt, Heiko & Klein, Marten 2023 Modeling simultaneous momentum and passive scalar transfer in turbulent annular poiseuille flow. *PAMM* **22** (1), e202200272.